HHS Public Access

Author manuscript

Cancer Cell. Author manuscript; available in PMC 2018 September 11.

Published in final edited form as:

Cancer Cell. 2017 September 11; 32(3): 310–323.e5. doi:10.1016/j.ccell.2017.08.002.

LMO1 Synergizes with MYCN to Promote Neuroblastoma Initiation and Metastasis

Shizhen Zhu[1,12,13,*], **Xiaoling Zhang**[1,13], **Nina Weichert-Leahey**[2,14], **Zhiwei Dong**[1,14], **Cheng Zhang**[3], **Gonzalo Lopez**[4], **Ting Tao**[2], **Shuning He**[2], **Andrew C. Wood**[5], **Derek Oldridge**[4], **Choong Yong Ung**[3], **Janine H. van Ree**[1], **Amish Khan**[1], **Brittany M. Salazar**[1], **Edroaldo Lummertz da Rocha**[3], **Mark W. Zimmerman**[2], **Feng Guo**[2], **Hong Cao**[1], **Xiaonan Hou**[6], **S. John Weroha**[6], **Antonio R. Perez-Atayde**[7], **Donna S. Neuberg**[8], **Alexander Meves**[9], **Mark A. McNiven**[1], **Jan M. van Deursen**[1], **Hu Li**[3], **John M. Maris**[4,10,11], and **A. Thomas Look**[2,*]

[1]Department of Biochemistry and Molecular Biology, Mayo Clinic College of Medicine, Mayo Clinic Cancer Center, Rochester MN, 55902, USA [2]Department of Pediatric Oncology, Dana-Farber Cancer Institute, Harvard Medical School, Boston MA, 02115, USA [3]Department of Molecular Pharmacology & Experimental Therapeutics, Center for Individualized Medicine, Mayo Clinic College of Medicine, Rochester, MN, 55902, USA [4]Division of Oncology and Center for Childhood Cancer Research, Children's Hospital of Philadelphia, Philadelphia PA, 19104, USA [5]Department of Molecular Medicine, University of Auckland, Auckland, New Zealand [6]Departments of Oncology, Radiation Oncology, and Molecular Pharmacology and Experimental Therapeutics, Mayo Clinic, Rochester, MN, 55902, USA [7]Department of Pathology, Children's Hospital Boston, Harvard Medical School, Boston MA, 02115, USA [8]Department of Biostatistics and Computational Biology, Dana-Farber Cancer Institute, Boston MA, 02215, USA [9]Department of Dermatology, Mayo Clinic, Rochester, MN, 55902, USA [10]Department of Pediatrics; Perelman School of Medicine at the University of Pennsylvania, Philadelphia, Pennsylvania PA, 19104, USA [11]Abramson Family Cancer Research Institute, Philadelphia, PA, 19104, USA

Summary

A genome-wide association study identified *LMO1*, which encodes a LIM-domain-only transcriptional cofactor, as a neuroblastoma susceptibility gene that functions as an oncogene in high-risk neuroblastoma. Here we show that *dβh* promoter-mediated expression of LMO1 in zebrafish synergizes with MYCN to increase the proliferation of hyperplastic sympathoadrenal precursor cells, leading to a reduced latency and increased penetrance of neuroblastomagenesis. The transgenic expression of LMO1 also promoted hematogenous dissemination and distant

[*]Correspondence: Zhu.shizhen@mayo.edu (S.Z.) (lead contact) and Thomas_Look@dfci.harvard.edu (A.T.L.).
[12]Lead Contact
[13]These authors contributed equally to this work
[14]These authors contributed equally to this work

Author Contributions: S.Z. and A.T.L designed the study, S.Z., A.T.L and N.W. wrote the manuscript; S.Z, X.Z., N.W., Z.D., T.T., S.H., M.Z., A.K, B.S. and F.G. performed the zebrafish experiments; G.L., A.C.W., D.O. and J.M.M. collected clinical information and analyzed GWAS data; A.R.P. performed the pathology analysis; D.S.N. performed statistical analyses; C.Z., E.L.R., C.Y.U and H.L. performed computational analyses; H.C., X.H, S.J.W. and M.A.M. assisted with the metastasis assays; A.M. assisted with immunohistochemical staining; J.H.v.R. and J.M.v.D. assisted with the live imaging.

Competing Financial Interests: The authors declare no competing financial interests.

metastasis, which was linked to neuroblastoma cell invasion and migration, and elevated expression levels of genes affecting tumor cell-extracellular matrix interaction, including *loxl3*, *itga2b*, *itga3* and *itga5*. Our results provide *in vivo* validation of *LMO1* as an important oncogene that promotes neuroblastoma initiation, progression, and widespread metastatic dissemination.

Graphical abstract

High expression of LMO1 is associated with neuroblastoma (NB) metastases. Zhu et al. show that LMO1 synergizes with MYCN to promote NB development and metastasis in zebrafish and that LMO1 elevates expression of genes affecting tumor cell-extracellular matrix interaction and promotes NB cell invasion.

Keywords

neuroblastoma; zebrafish model; metastasis; tumorigenesis; *LMO1*; *MYCN*

Introduction

Neuroblastoma is the most common extracranial solid tumor in children (Brodeur, 2003; Maris, 2010), accounting for 7% of all malignancies and 10% of cancer-related deaths in this age group (Park et al., 2013). It is derived from the developing sympathoadrenal (SA) lineage of neural crest cells, which give rise to the peripheral sympathetic nervous system (PSNS). The most common site of primary tumors is in the adrenal medulla (~45% of patients) with tumors also arising within ganglia along the sympathetic chain in the neck, chest, abdomen and pelvis (Maris, 2011; Park et al., 2013). Neuroblastoma is highly metastatic with about half of all affected children having distant metastasis to the bone marrow, cortical bone, noncontiguous lymph nodes, and liver (Maris et al., 2007). Long-term survival rates for high-risk neuroblastoma patients remain less than 40%, even with intensive treatment including multiagent chemotherapy, surgery, high-dose myeloablative therapy with autologous hematopoietic stem cell rescue, retinoids, and GD2-directed immunotherapy (Park et al., 2013).

Amplification of *MYCN* is present in about 20% of cases of neuroblastoma and is significantly associated with a poor outcome (Brodeur, 2003; Maris et al., 2007). Aside from *MYCN*, the next most frequently mutated gene in high-risk neuroblastoma is *ALK*, with inherited activating mutations of the kinase identified in ~1% of cases and acquired somatic mutations in 14% of all high-risk cases (Bresler et al., 2014; Pugh et al., 2013). Transgenic animal models of neuroblastoma, characterized by *dβh* promoter-mediated expression of *MYCN* and activated *ALK*, faithfully recapitulate the features of high-risk neuroblastoma, including its molecular pathology (Berry et al., 2012; Heukamp et al., 2012; Zhu et al., 2012). We have used a zebrafish model to show that activated ALK synergizes with MYCN by blocking a developmentally-timed apoptotic response that typically occurs in MYCN-overexpressing sympathoadrenal precursors (Zhu et al., 2012), opening the way for analysis of other oncogenes that potentiate the activity of MYCN during neuroblastoma pathogenesis.

Using a genome-wide-association study (GWAS) approach, we have shown that common polymorphic alleles at the LIM-domain-only gene (*LMO1*) locus are markedly enriched in neuroblastoma patients in general, with further enrichment in patients with metastatic disease, advanced age, an unfavorable pathological grade and a high-risk status (Wang et al., 2011). *LMO1* is a member of a family of transcriptional cofactor genes that encode two zinc-finger LIM domains, forming protein-protein interaction domains (Bach, 2000; Matthews et al., 2013). Depletion of LMO1 was cytotoxic to neuroblastoma cells harboring the risk haplotype, suggesting that this cofactor functions as a dominant oncogene in neuroblastoma cells (Wang et al., 2011). Recently, we have demonstrated that a polymorphism in the first intron of *LMO1* influences neuroblastoma susceptibility through differential GATA transcription factor binding. The allele that promotes high-risk neuroblastoma contains a GATA binding motif in this position, which results in a large super-enhancer driving high levels of *LMO1* expression, leading to an oncogenic dependency in tumor cells. In human populations, a protective allele, TATA, blocks formation of the super-enhancer and results in dramatically lower levels of *LMO1* expression and a significantly lower risk of developing neuroblastoma (Oldridge et al., 2015).

Results

LMO1 synergizes with MYCN in neuroblastomagenesis

To investigate the role of LMO1 in the pathogenesis of neuroblastoma in a vertebrate experimental system, we generated transgenic zebrafish lines that stably express human LMO1 in the PSNS under control of the zebrafish dopamine-β-hydroxylase gene (*dβh*) promoter. Two transgenic constructs, the *dβh:LMO1* and the *dβh:mCherry*, were coinjected into zebrafish embryos at the one-cell stage of development, so that these two transgenes would cointegrate in the transgenic fish (Langenau et al., 2008), aiding in the visualization of tumor development *in vivo*. Two transgenic lines expressing both the LMO1 and mCherry transgenes were identified and designated “LMO1” (Figures 1A, 1B, and S1A).

Although *LMO1* expression is upregulated in high-risk neuroblastomas due to an inherited regulatory single nucleotide polymorphism (SNP) and somatic copy number gains (Wang et al., 2011), tumors did not develop over 6 months in either of our fish lines with transgenic expression of LMO1 alone (Figure 1A). This is expected for a gene identified by GWAS that requires cooperating events to induce neuroblastomagenesis (Wang et al., 2011). To determine whether endogenous *lmo1* expression is dynamically regulated during PSNS development at the neuroblastoma initiation stage, we performed quantitative RT-PCR analyses on sorted control mCherry-expressing PSNS cells or LMO1-expressing cells from transgenic fish at 2 and 5.5 weeks of age. Interestingly, we found that endogenous *lmo1* is expressed at similar levels in sorted PSNS cells from control *dβh:mCherry* and LMO1 transgenic fish at both 2 weeks of age and 5.5 weeks of age (Figure S1B), suggesting that endogenous *lmo1* is expressed at a constant level during this window of PSNS cell development. In addition, the expression of human LMO1 transgene in the sorted PSNS cells from LMO1 transgenic fish but not the control *dβh:mCherry* transgenic fish was confirmed by quantitative RT-PCR (Figure S1C). Therefore, we hypothesize that permissive

polymorphisms lead to relatively constant high levels of *LMO1* expression in the PSNS cells, accounting for the influence of these polymorphisms on neuroblastoma susceptibility.

Given the strong association of *LMO1* and *MYCN* expression levels in high-risk neuroblastoma without *MYCN* amplification (Figures 1C and S1D), we next tested whether high levels of *LMO1* expression cooperate with MYCN to affect the onset and penetrance of neuroblastoma. Of note, our transgenic zebrafish model of neuroblastoma was developed to express MYCN under control of the *dβh* promoter and thus represents a model of high levels of MYCN expression in the absence of gene amplification.

After interbreeding LMO1 and MYCN transgenic fish, we observed tumor development in 80% of the MYCN;LMO1 progeny by 24 weeks of age, compared to an overall penetrance of 20-30% for the fish with MYCN expression alone (Figure 1A, $p<0.0001$). Thus, our results support the original prediction based on GWAS studies of children with neuroblastoma: that high levels of *LMO1* expression contribute to the initiation of neuroblastoma *in vivo*.

To examine whether transgenic expression of MYCN or MYCN plus LMO1 might affect endogenous *dβh* expression, we performed quantitative RT-PCR analysis on the sorted mCherry$^+$ PSNS cells from adult control *dβh:mCherry* transgenic fish and EGFP$^+$ tumor cells from MYCN-only and MYCN;LMO1 transgenic fish. As shown in the Figure S1E, endogenous *dβh* expression is significantly upregulated in both MYCN-only and MYCN;LMO1 tumor cells compared to that in the control PSNS cells, suggesting that expression of this gene is upregulated directly or indirectly by MYCN. Expression levels of *dβh* are similar in MYCN-only and MYCN;LMO1 neuroblastoma cells, indicating that differences in time of onset, penetrance and metastatic potential of the neuroblastomas between these two transgenic lines are not due to differences in the *dβh* expression levels.

Transgenic expression of LMO1 promotes hyperplasia of sympathoadrenal cells in the IRG

We previously showed that transgenic expression of MYCN alone induces sympathoadrenal neuroblast hyperplasia in the zebrafish IRG at 5 weeks of age (Zhu et al., 2012). However, the penetrance of neuroblastoma in transgenic fish expressing MYCN alone was low, resulting from a wave of apoptosis beginning at 5.5 weeks of age that removed the hyperplastic cells. Since this developmentally timed apoptotic response could be blocked by ectopic expression of activated ALK (Zhu et al., 2012), we asked whether the role of LMO1 in collaboration with MYCN differs from that of activated ALK in neuroblastoma pathogenesis.

Figure 2 shows the results of immunohistochemical analyses of fish with transgenic expression of LMO1 or controls. In sagittal sections through the IRG of 5-week-old transgenic fish expressing LMO1 alone, the number of mCherry$^+$ sympathoadrenal cells was similar to that of control *dβh:mCherry* transgenic fish, indicating that expression of LMO1 alone does not affect the numbers of sympathoadrenal cells at 5 weeks of age (Figures 2A and 2B). By contrast, MYCN and MYCN;ALK fish had ~50% more GFP$^+$ sympathoadrenal cells than the mCherry$^+$ cells in control fish (Figures 2A and 2B). However, MYCN;LMO1 transgenic fish had even more markedly increased numbers of GFP$^+$ or mCherry$^+$

sympathoadrenal cells compared to MYCN-only and MYCN;ALK fish, indicating a much faster neuroblast growth rate in MYCN;LMO1 transgenic fish (Figures 2A and 2B). Indeed, coexpression of LMO1 and MYCN resulted in markedly increased numbers of MYCN-expressing cells in nearly every fish at 5 weeks, consistent with the rapid onset and high penetrance of disease in MYCN;LMO1 transgenic fish.

To directly test whether the increased numbers of GFP^+/$mCherry^+$ sympathoadrenal cells in the transgenic fish coexpressing MYCN and LMO1 at 5 weeks of age reflect increased proliferation, we performed EdU pulse-labeling experiments in the control *dβh:EGFP*, MYCN, LMO1, and MYCN;LMO1 transgenic fish. In the control *dβh:EGFP* animals, there was very little EdU incorporation into GFP^+ sympathoadrenal cells in the IRG after 2 hours of EdU pulse-labeling (Figures S2 and 2C). The fraction of EdU-incorporating GFP^+ sympathoadrenal cells was significantly increased in the transgenic fish coexpressing MYCN and LMO1 as compared to those expressing MYCN alone or LMO1 alone (Figures S2 and 2C). These results indicate that transgenic expression of LMO1 synergizes with MYCN to induce neuroblastoma by increasing the proliferation of hyperplastic sympathoadrenal cells in the IRG.

To determine whether transgenic expression of LMO1 can rescue the MYCN-induced developmentally-timed apoptotic response in the IRG at 5.5 weeks of age, we assessed the expression of activated Caspase-3 as an indicator of apoptotic cell death. In 4 of 10 transgenic fishes expressing MYCN alone, we identified apoptotic sympathoadrenal cells coexpressing activated Caspase-3 and GFP in the IRG (Figure S3A and S3B). A similar number of MYCN;LMO1 transgenic fish showed activated $Caspase\text{-}3^+$, GFP^+ and $mCherry^+$ apoptotic sympathoadrenal cells in the IRG region (Figure S3A and S3B), suggesting that transgenic expression of LMO1 does not rescue MYCN-induced developmentally-timed apoptosis at 5.5 weeks of age. However, the total number of GFP^+ or $mCherry^+$ sympathoadrenal cells was significantly higher at 5.5 weeks of age in the fish coexpressing MYCN and LMO1 than in fish expressing MYCN alone (Figure S3C). Together, these findings suggest that the increased proliferation of sympathoadrenal cells caused by transgenic expression of LMO1 can overcome the MYCN-induced developmentally-timed apoptotic response at 5.5 weeks of age in the transgenic fish expressing both MYCN and LMO1. This, in turn, leads to the continued accumulation of the hyperplastic sympathoadrenal cells and highly penetrant and fully transformed neuroblastomas.

LMO1 collaborates with MYCN to promote metastases

Risk alleles within the *LMO1* locus leading to a predisposition for the development of neuroblastoma in children are associated with tumors expressing high levels of *LMO1* and an increased frequency of metastatic disease at diagnosis (Wang et al., 2011). Thus, we asked whether simultaneous expression of LMO1 and MYCN might promote tumor cell metastasis in our zebrafish model. For this analysis, we studied sagittal sections of MYCN, MYCN;LMO1, and MYCN;ALK transgenic fish at 5 to 7 months of age with GFP^+ tumors of similar size. Sections from five fish per group were examined by pathologist in a blinded fashion for the presence of metastatic disease. All of the primary tumors in these transgenic zebrafish lines arose in the IRG (Figures 3A, 3B, 3H, 3N, and S4A). These tumors were

composed of small, undifferentiated, and round tumor cells with hyperchromatic nuclei, often forming nests that were comparable histologically to the human neuroblastomas we described earlier (Zhu et al., 2012). Multifocal nests of tumor cells were also detected interspersed among the renal tubules in the transgenic fish in all genotypes expressing MYCN that developed tumors in the IRG (Figures 3A, 3C, 3I, 3O, and data not shown).

Strikingly, in three of five transgenic fish coexpressing MYCN and LMO1, we observed widespread tumor masses in multiple regions distant from the IRG and kidney, which were not observed in fish transgenic for MYCN-only or MYCN plus activated ALK (five fish per genotype, $p<0.05$, two-tailed probability by Fisher's exact test). Interestingly, each of these three fish harbored metastases in the orbit (Figures 3A, 3D, 3J, 3P and S4B), a metastatic site in children with neuroblastoma that is associated with a poor prognosis (Ahmed et al., 2006; Maris et al., 2007; Smith et al., 2010). We also identified metastases in the gill [functions in oxygen exchange, analogous to the mammalian lung (Menke et al., 2011)] (Figures 3A, 3E, 3K, 3Q and S4C) and spleen [analogous to the mammalian lymph node (Renshaw and Trede, 2012)] of transgenic fish expressing both MYCN and LMO1 (Figure 3A, 3F, 3L and 3R). Furthermore, in two fish, metastases were detected within the inner wall of the atrial chamber of the heart, an indication of hematogenous dissemination (Figures 3G, 3M, 3S and S4D). The metastatic tumor cells at all sites were readily detected by immunohistochemistry with the antibody against tyrosine hydroxylase (TH) (Figure 3H-M), which identified cells in the PSNS neuroblast lineage; the antibody against GFP (Figure 3N-S), which indicated cells expressing the transgenic MYCN-GFP fusion protein; and the antibody against LMO1 (Figure S4), which revealed cells expressing the human transgene. Of note, we observed similar levels of transgenic LMO1 protein expression in both primary tumors and metastatic tumor cells (Figure S4), suggesting that LMO1 expression levels are sufficient to optimally promote expression of downstream genes involved in enhanced invasion and migration without selection for higher expression levels in metastatic subclones. These findings indicate that transgenic expression of LMO1 in the PSNS of transgenic fish promotes the hematogenous dissemination of neuroblastoma, consistent with an association of the risk allele of *LMO1* with metastasis in high-risk neuroblastoma (Wang et al., 2011).

Increased LMO1 expression promotes the invasive and migratory properties of human neuroblastoma cells

Widespread hematogenous metastasis depends first on the ability of tumor cells to invade the surrounding stroma and migrate toward the blood stream (Clark and Vignjevic, 2015). To explore the effect of high levels of *LMO1* expression on the invasive and migratory properties of neuroblastoma cells, we first evaluated two *MYCN*-amplified human neuroblastoma cell lines with different levels of endogenous *LMO1* expression. We have previously shown that the Kelly neuroblastoma cell line has a G/- genotype at the rs2168101 locus, and that the G allele is associated with a functional GATA-binding site, leading to the formation of a super-enhancer that drives high levels of *LMO1* expression (Oldridge et al., 2015). By contrast, the BE2C cell line has a T/- genotype at this locus, and the T allele prevents formation of a functional GATA-binding site, leading to the lack of a strong enhancer and barely detectable *LMO1* expression (Oldridge et al., 2015). We first measured

the *LMO1* expression in these two cell lines by semi-quantitative RT-PCR and immunoblotting. These experiments confirmed that *LMO1* expression is significantly higher in the Kelly cell line than in the BE2C cell line at both mRNA (Figure 4A) and protein (Figure 4B) levels.

Next, we performed a transwell invasion and migration assay by culturing both Kelly and BE2C cell lines in serum-free media in the apical chamber over a collagen-coated transwell permeable membrane. The membrane is in contact with a lower basolateral chamber filled with media containing 10% FBS (Figure 4C). After 16 hours, the number of Kelly cells passing through the membrane was 3-fold higher than the BEC2 cell line as assessed by crystal violet staining of cells on the lower surface of the membrane (Figure 4D). Thus, the Kelly cell line with higher levels of *LMO1* expression has a greater ability to invade and migrate across a collagen-coated membrane. In addition, Kelly cells also migrated significantly faster than BE2C cells toward a region that had been scraped with a pipette along the bottom of the petri dish in a wound-healing assay (Figure 4E). These results indicate that Kelly cells with high levels of endogenous *LMO1* expression have increased invasive properties and higher levels of motility and greater migratory capacity than the BE2C cells with low levels of endogenous *LMO1* expression.

We then asked whether the lower levels of invasiveness, motility and migratory capacity of the BE2C cell line could be attributed to its low levels of *LMO1* expression. We transduced a MSCV-promoter-mediated LMO1 expression vector that also expresses GFP into the BE2C cells by retrovirus infection, enabling us to detect significantly higher levels of LMO1 expression in the infected BE2C cells by RT-PCR (Figure 5A) or by immunoblotting (Figure 5B). Compared to the vector-expressing control cells, stable overexpression of LMO1 significantly increased the numbers of cells that invaded and migrated across the collagen-coated membrane in the transwell assay (Figure 5C). The LMO1-expressing BE2C cells also migrated faster toward the lesion in a wound-healing assay in which the cells were treated with a proliferation inhibitor, mitomycin C (Di et al., 2015; McCarroll et al., 2004; Pullar et al., 2003), prior to the scratch assay, indicating that the accelerated wound healing is independent of cell proliferation (Figure 5D). We also detected faster random movement of BE2C cells stably expressing LMO1 than those expressing control vector when grown as monolayers *in vitro* (Figure 5E). These data indicate that increased levels of LMO1 expression can augment the invasiveness, motility and migratory capacity of BE2C cells, establishing the role of LMO1 in promoting these critical components of the metastatic phenotype.

To further evaluate whether silencing LMO1 can attenuate the invasiveness and migratory capacity of neuroblastoma cell lines with endogenous high levels of *LMO1* expression, we first knocked down LMO1 expression in two neuroblastoma cell lines, Kelly (G/-; *MYCN* amplified) (Figure 4A) and SHEP-Tet/21N (G/G; *MYCN* nonamplified with a doxycycline regulated Tet-off MYCN expression vector) (Lutz et al., 1996) (Figure S5A), using the lentiviral-based shRNA that has been successfully used to knock down LMO1 expression in a previous study (Wang et al., 2011). In contrast to cells infected with scrambled control lentiviral shRNA, Kelly cells (Figure S5B) and SHEP-Tet/21N cells treated with doxycycline to silence MYCN expression (Figure S5C and S5D) underwent rapid cell death

after LMO1 lentiviral shRNA infection, in agreement with previous reports that *LMO1* expression is required for tumor cell survival in neuroblastomas with permissive risk alleles (Oldridge et al., 2015; Wang et al., 2011). Due to dramatically reduced numbers of tumor cells after LMO1 knockdown, we were unable to perform cell invasion and migration assays after LMO1 knockdown in these lines.

Molecular pathways altered by increased LMO1 expression

To identify key genes affected by increased *LMO1* expression, we first used RNA sequencing to interrogate global gene expression profiles in BE2C cells expressing LMO1 or a control vector. By Gene Set Enrichment Analysis (GSEA), the LMO1-expressing BE2C cells showed enrichment for a gene signature encoding “matrisome-associated proteins” (Figure 6A), which consists of structural extracellular matrix (ECM) proteins together with ECM-associated enzymes (Hynes and Naba, 2012; Naba et al., 2012). Also enriched in LMO1-expressing BE2C cells were the related gene signatures for “ECM regulators” (Figure 6B) and “integrins” (Figure 6C). We also performed transcriptome analyses between Kelly cells (expressing high levels of endogenous *LMO1*) and BE2C cells (expressing low levels of endogenous *LMO1*). Finally, there was robust enrichment of the signature of genes encoding “matrisome”, “extracellular matrix”, and “integrin” in Kelly cells compared to BE2C cells by GSEA (Figure S6A-C).

To extend this analysis, we examined expression levels of the representative enriched genes from these datasets. Using quantitative RT-PCR analyses of both human neuroblastoma cell lines and zebrafish neuroblastomas, we detected increased expression of *LOXL3*, *ITGA2B*, *ITGA3*, and *ITGA5* in BE2C cells overexpressing LMO1 (Figure 6D) and Kelly cells (Figure 6E). In addition, we also detected downregulation of these candidate genes in Kelly cells infected with LMO1 lentiviral-shRNA as compared to those infected with control shRNA (Figure S6D), indicating that these genes are important downstream targets of LMO1. To examine the expression association of these genes with *LMO1* in primary neuroblastomas, we analyzed publically available microarray data and found a significant correlation between expression levels of *LMO1* and all of the aforementioned genes in Stage 4 neuroblastomas with single-copy *MYCN* (Figure 6F), further supporting that these genes are indeed crucial LMO1 target genes that contribute to neuroblastoma dissemination. The zebrafish homologues of these representative genes were also upregulated in zebrafish neuroblastomas cells expressing transgenic LMO1 and MYCN vs. those expressing MYCN alone (Figure 7A), supporting the idea that ECM-associated genes secreted by the neuroblastoma cells with high levels of LMO1 expression contribute to the increased hematogenous dissemination and widespread metastasis in MYCN;LMO1 transgenic fish.

Among the upregulated ECM-associated genes, those in the lysyl oxidase (LOX) family encode enzymes that crosslink collagen, leading to increased matrix stiffness and promoted cancer cell invasion (Kagan and Li, 2003; Smith-Mungo and Kagan, 1998). To determine whether collagen deposition within neuroblastoma is affected by upregulated *LOX* family genes in LMO1-expressing tumors, we performed staining on the paraffin sections from three MYCN-only and three MYCN;LMO1 tumors with picrosirius red (PSR), a highly selective and widely used stain for collagen fibers to assess collagen deposition and ECM

stiffness (Junqueira et al., 1978; Sweat et al., 1964). This assay showed significantly increased numbers of PSR-stained collagen fibers, which also form thicker bundles, in the tumors expressing both MYCN and LMO1, compared to the tumors expressing MYCN alone (Figure 7B-F). These results support our findings that upregulation of ECM-associated genes driven by high levels of LMO1 expression lead to increased collagen deposition and remodeling of the matrix in ways that increase ECM stiffness and facilitate tumor cell dissemination.

To further investigate whether suppression of LOX enzymatic activity could abolish the enhanced invasive and migratory capacity of BE2C cells with stable overexpression of LMO1, we treated the LMO1- or vector-expressing BE2C cells with an irreversible inhibitor of LOX enzymes, β-aminopropionitrile (BAPN). In the control vector-expressing BE2C cells, BAPN treatment did not change the numbers of cells that invaded and migrated across the collagen-coated membrane in the transwell assay (Figure 7G and 7H). By contrast, the numbers of LMO1-expressing BE2C cells passing through the membrane were significantly reduced in the BAPN treated group compared to the control untreated group (Figure 7G and 7H). In addition, the monoamine oxidase assay showed that the LOX activity was significantly reduced in both LMO1-and vector-expressing BE2C cells treated with the BAPN (Figure 7I). Hence, these findings support our findings that members of the LOX family are critical downstream targets of LMO1, which contribute to metastasis in neuroblastoma by promoting tumor cell invasion and migration.

Discussion

Here we show that high levels of LMO1 expression cooperate with MYCN to accelerate the onset of neuroblastoma *in vivo* and markedly increase its penetrance. These results provide independent support in an animal model for recent GWAS findings implicating *LMO1* as a neuroblastoma susceptibility gene whose high levels of expression promote the initiation of neuroblastoma in high-risk patients (Wang et al., 2011). We also provide evidence that LMO1 acts synergistically with MYCN to promote increased proliferation of hyperplastic sympathoadrenal precursor cells in the IRG. LMO1 belongs to a family of transcriptional cofactors that act as bridges to link master transcription factors together to control cell state during development, leading to the formation of large enhancers that are themselves further amplified by interacting with MYC family proteins. Importantly, transgenic expression of LMO1 also promotes hematogenous dissemination of neuroblastoma in the form of multiple distant metastases in transgenic zebrafish that also overexpress MYCN. As shown in this report, the mechanism for this effect appears to be the upregulation of genes associated with the ECM, providing insight into the connection between high levels of *LMO1* expression and widespread metastasis in human neuroblastomas (Wang et al., 2011).

In our RNA-sequencing and GSEA analyses, we found that the gene signature defined as “matrisome-associated-proteins” is significantly enriched in the BE2C cells with stable overexpression of LMO1 and the Kelly cells with high levels of endogenous *LMO1* expression. The “matrisome” consists of ECM proteins (core matrisome) and associated factors (matrisome-associated proteins), as first defined by Hynes and colleagues based on *in silico* analysis of genes encoding ECM-associated proteins (Hynes and Naba, 2012; Naba et

al., 2012). Representative enriched genes from these processes, including *LOXL3*, *ITGA2B*, *ITGA3*, and *ITGA5*, were significantly upregulated in both human neuroblastoma cell lines and zebrafish neuroblastomas with increased levels of LMO1 expression, suggesting that the dynamic remodeling of the ECM might be involved in LMO1-induced tumor metastasis.

The ECM supports cell proliferation, survival, differentiation, and migration by providing architectural support and biophysical/biochemical cues (Hay, 1981; Hay, 1989). Tumor-associated ECM remodeling, such as increased collagen deposition, fiber alignment and crosslinking, results in increased ECM stiffness and mechanical force, leading to enhanced metastasis (Levental et al., 2009; Paszek et al., 2005). The *LOX* family, including LOX and LOX-like 1-4 genes, encode secreted copper-dependent amine oxidases that are the key regulators for cross-linking of collagen and elastin and stiffening of cancer tissue (Kagan and Li, 2003; Smith-Mungo and Kagan, 1998). Elevated expression of *LOX* family genes has been reported to be associated with invasion and metastasis of high-grade tumors of various cancer types (Hoye and Erler, 2016; Naba et al., 2012), including breast (Erler et al., 2006; Kirschmann et al., 2002), colorectal (Baker et al., 2011), prostate (Lapointe et al., 2004), hepatocellular carcinoma (Wong et al., 2014) and head and neck cancers (Barker et al., 2012). Consistent with this mechanism, we found that a member of the lysyl oxidase family genes, *LOXL3*, is significantly upregulated in the BE2C cells with stable overexpression of LMO1, and Kelly cells with endogenous high levels of *LMO1* expression, as well as neuroblastomas arising in MYCN;LMO1 transgenic fish. We also observed significantly increased numbers of PSR-stained collagen fibers, suggesting increased deposition of collagen in the zebrafish tumors coexpressing MYCN and LMO1. Hence, these findings suggest that the remodeling of tumor microenvironment by upregulated ECM regulators, including increased deposition of collagens and augmented stiffness of the ECM induced by LOX family members, might facilitate LMO1-induced neuroblastoma invasion and metastasis.

Moreover, ECM stiffness can promote focal adhesion assembly, which also enhances cell migration. Focal adhesions are membrane-associated multiprotein complexes that form mechanical links between intracellular actin bundles and the extracellular substrate through integrins, which are transmembrane glycoproteins (Hynes, 2002). Stiffened ECM can activate integrins to form heterodimers at the cell surface and subsequently the intracellular domain of integrins that bind to the cytoskeleton via adapter proteins, thus triggering signaling cascades that result in remodeling of the cytoskeleton (Miranti and Brugge, 2002). The dynamic assembly and disassembly of focal adhesions plays a central role in cell migration. We found that many members of the integrin family genes, such as *ITGA2B*, *ITGA3*, and *ITGA5*, were upregulated in LMO1-expressing BE2C cells, Kelly cells, and neuroblastomas in the transgenic fish-coexpressing MYCN and LMO1.

Upregulation of integrins has been shown to be associated with invasion and motility in many types of tumor cells (Ganguly et al., 2013). For example, integrin α5 acts downstream of *Runt*-related transcription factor 2 (RUNX2) and steroid receptor coactivator-1 (SRC-1) to promote breast cancer cell adhesion and metastasis to the bone (Li et al., 2016; Qin et al., 2011). A high *ITGA3/CD9* expression ratio is associated with a high rate of lymph node metastasis and invasive histopathology of oral squamous cell carcinoma (Nagata et al.,

2013), while enhanced ITGA3/ITGB1 signaling by downregulation of *miR-223* contributes to migration and invasion of PCa cancer cells (Kurozumi et al., 2016). In addition, high levels of *ITGA2B* expression have been shown to correlate with poor prognosis for overall survival of clear cell renal cell carcinoma (Lu et al., 2016). Taken together, these findings indicate that the increased cell migration in human neuroblastoma cell lines with high levels of LMO1 expression or tumor metastasis in transgenic fish coexpressing MYCN and LMO1 could be in part due to enhanced assembly of focal adhesion complex and rearrangement of actin cytoskeleton by upregulated integrins. Hence, our zebrafish model of neuroblastoma with coexpression of LMO1 and MYCN should provide a valuable platform for evaluating the effect of integrin inhibitors to prevent or inhibit neuroblastoma metastasis *in vivo* (Dennis et al., 1990; Hartman et al., 1992; Neely et al., 2010; Tcheng et al., 2001).

Our results suggest a model of the underlying molecular mechanisms that explain the synergy between LMO1 and MYCN in neuroblastoma metastasis (Figure 8). Very briefly, LMO1 upregulates the expression of ECM regulatory genes, leading, in turn, to remodeling of the extracellular matrix, assembly of focal adhesion complexes and rearrangement of the actin cytoskeleton, which together result in enhanced invasion, motility and metastasis of cells with high levels of LMO1 expression. It will be important in the future to extend these studies to investigate *in vivo* how neuroblastoma cells with high levels of *LMO1* expression interact with the microenvironment to promote metastasis. Our studies provide mechanisms through which LMO1 expression driven by the risk G allele contributes to tumor invasion and dissemination, which remain as major problems in two-thirds of children with high-risk forms of this disease.

Contact for Reagent and Resource Sharing

Further information and requests for resources and reagents should be directed to and will be fulfilled by the Lead Contact, Shizhen Zhu (zhu.shizhen@mayo.edu).

Experimental Model and Subject Details

Cell Lines and Cell Culture

The human neuroblastoma Kelly cell line was obtained from Sigma-Aldrich; the neuroblastoma BE2C cell line was obtained from the American Type Culture Collection (ATCC); the neuroblastoma SHEP-Tet/N21 cell line was a generous gift from Dr. M. Schwab at the German Cancer Research Center, Heidelberg, Germany (Lutz et al., 1996). These human neuroblastoma cell lines were cultured in RPMI 1640 medium (Gibco 22400) supplemented with 10 % (v/v) fetal bovine serum (FBS) (Gibco, 26140079), penicillin (100 U/ml), and streptomycin (100 mg/ml) at 37°C with 5% CO_2. Medium was changed once every two days. The cell lines were authenticated by ATCC using STR profiling.

Animal models

Zebrafish were all of the AB background strain. Embryos were staged according to Kimmel et al. (Kimmel et al., 1995). All zebrafish studies and maintenance of the animals were in accord with Dana-Farber Cancer Institute IACUC-approved protocol #02-107 and Mayo Clinic IACUC-approved protocol # A41213.

Method Details

DNA constructs for transgenesis

To generate *dβh:LMO1* DNA constructs for the *Tg(dβh:LMO1),Tg(dβh:mCherry)* transgenic lines, we first amplified the coding region of human LMO1 using PCR with following program:1 cycle of 94 °C for 2 min, followed by 30 cycles of (94°C, 30 sec, 55°C, 30 sec, 72°C, 1 min),72°C, 7 min (forward LMO1 ATTB1 primer: 5′-GGGGACAAGTTTGTACAAAAAAGCAGGCTACACCATGATGGTGCTGGACAAGGAGGA-3′ and reverse LMO1 ATTB2 primer: 5′-GGGGACCACTTTGTACAAGAAAGCTGGGTTTACTGAACTTGGGATTCAAAGGT-3′). The PCR product was cloned into the *pDONR221* gateway donor vector by BP reaction. Then, the expression construct was generated by combining three entry clones --- *dβh-pDONRP4-P1R, LMO1-pDONR221* and *p3E-polyA*--- with a modified destination vector containing *I-SceI* recognition sites using the multisite Gateway system (Invitrogen, CA) (Zhu et al., 2012). The *dβh:mCherry* DNA construct was generated with the Multisite Gateway System by combining entry clones of a 5.2-kb *dβh* promoter (Zhu et al., 2012), *pME-mCherry* and *p3E-polyA* into the modified destination vector containing *I-SceI* recognition sites.

To generate stable lines that overexpress LMO1 in the PSNS, we linearized the *dβh:LMO1* DNA construct and the *dβh:mCherry* DNA construct (3:1 ratio) with the *I-SceI* enzyme. Total DNA (50-80 pg) was then injected into one-cell-stage wild-type embryos. The *Tg(dβh:LMO1),Tg(dβh:mCherry)* zebrafish line is designated the “LMO1” transgenic line in the main body of text. F1 offspring were first screened by fluorescent microscopy for mCherry expression, and the germline transmission of the LMO1 gene was confirmed by genomic PCR of the mCherry^{+} embryos using the following primers: LMO1 FW1: 5′-GATGGTGCTGGACAAGGAGGACGGCG-3′ and LMO1 RV: 5′-GGTGCCATTGAGCTGCCCTTCCT-3′ and the following PCR program: 1 cycle of 94°C for 5 min, 30 cycles of (94°C for 30 s, 55°C for 30 s, and 72°C for 60 s). A 450-bp fragment of the LMO1 transgene fragment was amplified and confirmed by sequencing. A portion of the linearized *dβh:mCherry* DNA construct (50-80 pg) was injected into one-cell-stage wild-type embryos to develop stable transgenic line overexpressing mCherry alone in the PSNS.

Tumor watch and genotyping of transgenic fish

MYCN and LMO1 heterozygous transgenic fish were interbred, and the offspring were grown under identical conditions and then screened every 2 weeks, starting from 5 weeks postfertilization (wpf) for fluorescent EGFP- or mCherry-expressing cell masses indicative of tumors. Fish with tumors were separated, genotyped and analyzed further by H&E staining and immunohistochemical assays. For genotyping, genomic DNA extracted from finclips was PCR-amplified with the following primers: LMO1 FW1: 5′-GATGGTGCTGGACAAGGAGGACGGCG -3′; LMO1 RV: 5′-GGTGCCATTGAGCTGCCCTTCCT -3′; MYCN-test F1: 5′-CTG CTT GAG AAC GAG CTG TG-3′; and MYCN-R3: 5′-AGG CAT CGT TTG AGG ATC AG-3′. LMO1 genotyping PCR was performed with Taq DNA Polymerase (New England Biolabs, MA) using the program described above, while MYCN genotyping was performed with the GC-

RICH PCR System (Roche Applied Science, IN) using the following program: 1 cycle of 95°C for 3 min, 25 cycles of 95°C for 30 s, 58°C for 30 s, and 72°C for 3 min.

EdU pulse-labeling

For EdU pulse-labeling, 1 μl of 2.5 mg/ml Edu solution from the Click-iT Alexa Fluor 647 imaging kit (Life technologies, Cat# C10340) was injected retro-orbitally into anesthetized transgenic fish at 5 weeks of age. Two hours after injection, the fish were fixed for cryosectioning according to the protocol below, with immunostaining according to the manufacturer's protocol.

Cryosectioning

Embryos or juvenile fish at indicated stages were fixed with 4% paraformaldehyde at 4°C overnight, washed with phosphate-buffered saline with 0.1% Tween 20 (PBST), embedded in 1.5% agar / 5% sucrose, and sunk in 30% sucrose at 4°C overnight. Sagittal sections (12 μm each) through the whole fish were taken from the embedded specimens using a conventional cryostat.

Immunostaining and picrosirus red staining

For immunofluorescence assays, primary antibodies against GFP (Thermo Fisher Scientific, Cat# A6455, 1:500; and Cat# A11120, 1:500) and activated Caspase-3 (BD Biosciences, Cat# 559565, 1:250) were incubated on slides at 4°C overnight, washed with PBST, visualized with secondary antibodies conjugated with Alexa 488, 633 or 647 (Thermo Fisher Scientific, 1:500), and counterstained with DAPI for nuclear staining.

Paraffin sectioning followed by H&E staining was performed at the DF/HCC or Mayo Clinic Research Pathology Core. Immunohistochemistry of paraffin sections was performed using a Leica BOND-MAX instrument and BONDTM reagents with primary antibodies against TH (Pel-Freez, Cat# P40101, 1:500), GFP (Thermo Fisher Scientific, Cat# A6455, 1:500) and LMO1 (Abcam, Cat# ab84456, 1:250) using standard protocols. Collagen accumulation was detected by picrosirius red staining using the picrosirius red stain kit (Polysciences, 24901-250). The picrosirius red-positive collagen fibers were counted in at least three random fields for each section using ImageJ software.

Imaging

A Zeiss Lightsheet Z.1 microscope and a Leica MZ10F Stereo fluorescence microscope were used for capturing the bright field and fluorescent images of tumor fish. Confocal images of the $EGFP^+$, $mCherry^+$ or immunostained sections were collected with a Zeiss LSM 780 laser scanning confocal microscope at the Microscopy and Cell Analysis core facility at Mayo Clinic. For the bright-field images of H&E stained, picrosirius red stained or immunostained paraffin sections, we used an Olympus AX70 compound microscope equipped with an Olympus DP71 camera. For the wound-healing assay, 10× phase-contrast images were acquired every 2 hours over a 24-26 hours period using a Zeiss Observer. Z1 microscope equipped with an AxiaCam MRm camera. At least 10 representative fields per well were imaged. The acquired images were processed and compiled with Zeiss ZEN 2012,

Leica Application Suite X (v. 2.0.0), Adobe Photoshop, Illustrator CS3 (Adobe), Image-Pro and Image J software.

Cell counts on sections

To analyze the development of the sympathoadrenal cells before tumor onset, the *dβh:mCherry*, LMO1, MYCN and MYCN;LMO1 transgenic fish were cryosectioned, stained with primary antibodies against GFP or activated Caspases-3 and imaged with confocal microscopy at 5 and 5.5 wpf. All sections from each individual fish were scanned, a single representative section containing the largest number of sympathoadrenal cells or activated Caspases-3 positive sympathoadrenal cells in the IRG was selected, and the resultant cell numbers were quantified.

To assess the proliferative capacity of the sympathoadrenal cells in the IRG of *dβh:EGFP*, MYCN, LMO1 and MYCN;LMO1 transgenic fish at 5 weeks of age, we cryosectioned the transgenic fish that had undergone 2-hour EdU pulse-labeling, followed by immuostaining with primary antibody against GFP and confocal imaging. A single representative section with the highest ratio of EdU^+ sympathoadrenal cells to the total number of GFP^+ or $mCherry^+$ sympathoadrenal cells in the IRG was selected, and the numbers of those cells were quantified.

Virus production and infection

The *MSCV-IRES-GFP* (*MIG*) retroviral expression vector containing LMO1 cDNA was a gift from Dr. Sanda Takaomi at the Cancer Science Institute of Singapore. The retroviral construct containing LMO1 or empty vector was co-transfected into 293T cells with packaging plasmid *pMD-MLVogp* and envelope plasmid *VsVg* using FuGENE 6 reagent (Roche). Supernatants containing the retrovirus were collected, filtered through a 0.45 μm filter and infected BE2C cells in the presence of polybrene (8 μg/mL). MSCV-promoter-mediated expression of LMO1 in the stable cell lines was verified by qRT-PCR and western blot analyses.

For LMO1 knockdown, Kelly and SHEP-Tet/N21 cells were infected with control scrambled shRNA lentiviral particles (Santa Cruz, sc-108080) or LMO1 shRNA (h) lentiviral particles (Santa Cruz, sc-38025-v). The infected cells were treated with puromycin (Sigma P9620) for 36 hours, and mRNA was harvested at 96 hours post infection to determine the level of LMO1 knockdown and the expression of candidate LMO1-target genes. The numbers of cells in 6-well plates were counted manually once every two days from day 3 to day 9 after infections. All the values were normalized to the numbers of infected cells at day 3 to generate the growth curve.

Transwell migration and invasion assay

5×10^4 cells were seeded on an insert coated with collagen (8 μm pore size) in the upper chamber with serum free medium. Media containing 10% fetal bovine serum was added to the lower chamber. After 16~20 hours of incubation, the cells remaining on the upper membrane were removed with cotton wool. The cells that had migrated through the membrane were fixed with 100% pre-chilled methanol, stained with crystal violet and

imaged using an Olympus AX70 compound microscope. At least 5 representative fields per membrane were imaged. Experiments were independently repeated three times.

For the LMO1 or vector-overexpressing BE2C cells subjected for the LOX inhibitor BAPN treatment, they were first incubated with 500 μM BAPN (A3134-5G, Sigma) for 24 hours and then seeded on an insert coated with collagen in the upper chamber with serum free medium. The cell culture supernatant was collected for measuring LOX activity using the Amplex Red Monoamine Oxidase Assay Kit (Life Technologies, A12214).

Wound-healing assay

1.5×10^5 cells were seeded in a well of 6-well plate and incubated for 24 hours to achieve 90-100% confluence. Sterile yellow pipette tips were used to create wounds. After being rinsed with phosphate-buffered saline (PBS) 3 times, cells were further cultured in RPMI 1640 medium supplemented with 10% FBS for 22-26 hours at 37°C. Assays were repeated three times for each cell line. Cells migrated into wound area were quantified by relative percentage of wound area covered by migrated cells to the original wound area. To distinguish the effect of migration from proliferation, LMO1 or vector-expressing BE2C cells were incubated with 20 μg/ml mitomycin C (Sigma M4287) for 2 hours prior to the scratch assay to inhibit proliferation.

Time-lapse microscopy and cell motility measurement

Neuroblastoma cells were sparsely seeded in single wells with a glass bottom. 10× phase-contrast time-lapse images were acquired every 30 minutes over 24 hours using a Zeiss Observer. Z1 microscope equipped with an AxiaCam MRm camera. At least 10 representative fields per well were imaged. Cell centroids of each cell throughout the time sequence were determined manually. A nearest neighbor algorithm (Huth et al., 2010) was applied to track cell movements.

Western blotting

Protein lysates were prepared from neuroblastoma cell lines in pre-chilled RIPA buffer (150 mM NaCl, 50 mM Tris-HCl pH 8, 5 mM EDTA, 50 mM PMSF, 1% Igepal CA 630, 0.5% sodium deoxycholate, 0.1% SDS and 1× Halt protease inhibitor cocktail). Protein concentrations were determined by Bradford assay (BioRad). About 80 μg of protein lysates were separated by 12% gel electrophoresis, transferred to PVDF membranes (Millipore) and probed overnight at 4°C with the following primary antibodies: anti-LMO1 (Bethyl Laboratories, 1:1000), anti-GFP (Abcam; ab6556, 1:5000), anti-β-ACTIN (Biolegend, Poly6221; 1:500). Primary antibody binding was visualized on X-ray film using anti-mouse-HRP (Cell Signaling 7076; 1:5000) or anti-rabbit-HRP (Cell Signaling 7074; 1:5000) secondary antibodies along with Pierce ECL western blotting substrate or SuperSignal West chemiluminescent substrates (Thermo Fisher Scientific).

RNA extraction and real-time PCR analysis

Total RNA was isolated from neuroblastoma cell lines (~ 10,000 cells), sorted PSNS cells or tumors of control *dβh:mCherry*, MYCN-only and MYCN;LMO1 transgenic fish using Trizol (Sigma-Aldrich). RNA was reverse-transcribed using Superscript™ III reverse

transcriptase (Thermo Fisher Scientific, Cat# 18080044) with oligo (dT) primer. The real-time PCR was performed using CFX96 Touch™ Real-Time PCR Detection System (BIO-RAD) with the SYBR Supermix (BIO-RAD). Sequences of primer sets are available in Supplemental table 1. All reactions were performed in triplicate. Quantitative data were calculated from the Ct-values for each reaction using the mean reaction efficiency for each primer pair. Data were normalized to the expression levels of *ACTIN* for human genes and the *elfa* for zebrafish genes, respectively.

Gene expression correlation analysis

The TARGET RNAseq cohort is available from the Sequence Read Archive (SRA) study (accession phs000467). Gene expression is quantified as transcripts per million (TPM) by using Kallisto (Bray et al., 2016). Multiple transcriptions were aggregated into gene expression level. The SEQC RNA-seq cohort is available from Gene Expression Omnibus (GEO), accession code GSE62564. Gene expression was quantified as Fragments Per Kilobase (FPKM) as described earlier (Wang et al., 2014). The TARGET HumanExon cohort is available from the data matrix portal (https://ocg.cancer.gov/programs/target/data-matrix). The NRC HumanExon microarray expression data is available from GEO, accession code GSE85047. The gene expression correlation between *LMO1* and *MYCN* was computed using the Spearman's rank correlation coefficient.

The Westermann-105-custom-ag44kcwolf microarray expression data is available from GEO, accession code GSE73517. Expression intensities were normalized using Robust-Multichip Analysis (RMA). High-risk cases are those categorized as Stage 4 (INSS) tumors in patients diagnosed older than 18 months old. The gene expression correlations between *LMO1* and *LOXL3*, *ITGA2B*, *ITGA3*, or *ITGA5* were computed using the Pearson correlation coefficient.

RNA-sequencing analysis

Fastq files containing paired RNA-seq reads were aligned using Tophat 2.0.14 software (Kim et al., 2013) and then analyzed against the UCSC hg19 reference genome using Bowtie 2.2.6 software (Langmead and Salzberg, 2012) with default settings. The gene counts from uniquely mapped, non-discordant read pairs were obtained using the subRead featureCounts program (v1.4.6) and these genes were annotated based on the UCSC hg19 Illumina iGenomes annotation package. Read counts were further normalized using size factors from the DESeq package (Anders and Huber, 2010). The data were then log2 transformed after the addition of +1 to all counts. The genes with log2 [nCounts+1]> 1 (~ 17577 genes) were subjected for differential expression analysis using the DESeq package.

Gene set enrichment analyses (GSEA)

Genes from whole transcriptomic data were ranked based on the fold changes of gene expression (in log2 scale) in LMO1-epxressing BE2C cells vs. vector-expressing Be2C cells, or Kelly cells vs. BE2C cells. Pre-ranked option of GSEA (Subramanian et al., 2005) was performed using canonical pathway (CP) gene signatures with 1000 permutations for statistical evaluation. Curated genesets (CP) corresponding to canonical pathways (1330

pathways) under C2 category in MSigDB (http://software.broadinstitute.org/gsea/msigdb/index.jsp) were used. Pathways with nominal p value <0.05 were deemed enriched.

Quantification and Statistical Analysis

Statistical analysis was performed using GraphPad Prism software version 5.0 (La Jolla, CA). The method of Kaplan and Meier was used to estimate the rate of tumor development. Fish that died without evidence of $EGFP^+$ or $mCherry^+$ masses were censored. The log-rank test was used to assess differences in the cumulative frequency of neuroblastoma between MYCN-only transgenic fish and MYCN;LMO1 transgenic fish. To address the possibility of unequal variances, the Welch t-test followed by the Bonferroni correction was used to compare the differences between two groups in fish studies. One-way ANOVA with Tukey's post-hoc test was performed to compare the differences among groups in cell line studies. Unpaired t-test (two-tailed) was used when two groups were compared. For all experiments with error bars, the standard error of the mean was calculated and the data were presented as mean ± SD. The sample size for each experiment and the replicate number of experiments were included in the figure legends.

Data and Software Availability

All RNA-sequencing data generated in this study have been deposited in the GEO under ID code GSE90087.

Supplementary Material

Refer to Web version on PubMed Central for supplementary material.

Acknowledgments

We thank J.R. Gilbert for editorial review of the manuscript and critical comments. This work was supported by a grant R00CA178189 (S.Z.) from the National Cancer Institute; a grant W81XWH-17-1-0498 (S.Z.) from the United States Department of Defense (DoD); young investigator awards from Alex's Lemonade Stand Foundation (S.Z.) and the CureSearch for Children's Cancer Foundation (S.Z.); a V Scholar award from the V Foundation for Cancer Research (S.Z.) and pilot project awards from the Fraternal Order of Eagles (S.Z.) and the Mayo Center for Biomedical Discovery (S.Z.); support from the Mayo Clinic Cancer Center, Center for Biomedical Discovery, and Center for Individualized Medicine (S.Z.); a grant R01 CA180692 (J.M.M and A.T.L.) from the National Cancer Institute; an Alex's Lemonade Stand Foundation Innovation Award (A.T.L.); a grant R01 CA124709 from the National Cancer Institute and an award from the Press On Foundation (J.M.M); a grant R01 CA196631-01A1 (H.L.) from the National Institutes of Health; a fellowship from the Friends for Life and the Friends of DFCI, a grant from the Children's Neuroblastoma Cancer Foundation (T.T.); a grant from the German Cancer Aid 110801 (N.W.); a fellowship from the Damon Runyon-Sohn Foundation (DRSG-9-14) (M.Z.).

References

Ahmed S, Goel S, Khandwala M, Agrawal A, Chang B, Simmons IG. Neuroblastoma with orbital metastasis: ophthalmic presentation and role of ophthalmologists. Eye (Lond). 2006; 20:466–470. [PubMed: 15895028]

Anders S, Huber W. Differential expression analysis for sequence count data. Genome biology. 2010; 11:R106. [PubMed: 20979621]

Bach I. The LIM domain: regulation by association. Mechanisms of development. 2000; 91:5–17. [PubMed: 10704826]

Baker AM, Cox TR, Bird D, Lang G, Murray GI, Sun XF, Southall SM, Wilson JR, Erler JT. The role of lysyl oxidase in SRC-dependent proliferation and metastasis of colorectal cancer. Journal of the National Cancer Institute. 2011; 103:407–424. [PubMed: 21282564]

Barker HE, Cox TR, Erler JT. The rationale for targeting the LOX family in cancer. Nature reviews Cancer. 2012; 12:540–552. [PubMed: 22810810]

Berry T, Luther W, Bhatnagar N, Jamin Y, Poon E, Sanda T, Pei D, Sharma B, Vetharoy WR, Hallsworth A, et al. The ALK(F1174L) mutation potentiates the oncogenic activity of MYCN in neuroblastoma. Cancer cell. 2012; 22:117–130. [PubMed: 22789543]

Bray NL, Pimentel H, Melsted P, Pachter L. Near-optimal probabilistic RNA-seq quantification. Nature biotechnology. 2016; 34:525–527.

Bresler SC, Weiser DA, Huwe PJ, Park JH, Krytska K, Ryles H, Laudenslager M, Rappaport EF, Wood AC, McGrady PW, et al. ALK Mutations Confer Differential Oncogenic Activation and Sensitivity to ALK Inhibition Therapy in Neuroblastoma. Cancer cell. 2014; 26:682–694. [PubMed: 25517749]

Brodeur GM. Neuroblastoma: biological insights into a clinical enigma. Nature reviews Cancer. 2003; 3:203–216. [PubMed: 12612655]

Clark AG, Vignjevic DM. Modes of cancer cell invasion and the role of the microenvironment. Current opinion in cell biology. 2015; 36:13–22. [PubMed: 26183445]

Dennis MS, Henzel WJ, Pitti RM, Lipari MT, Napier MA, Deisher TA, Bunting S, Lazarus RA. Platelet glycoprotein IIb-IIIa protein antagonists from snake venoms: evidence for a family of platelet-aggregation inhibitors. Proceedings of the National Academy of Sciences of the United States of America. 1990; 87:2471–2475. [PubMed: 2320569]

Erler JT, Bennewith KL, Nicolau M, Dornhofer N, Kong C, Le QT, Chi JT, Jeffrey SS, Giaccia AJ. Lysyl oxidase is essential for hypoxia-induced metastasis. Nature. 2006; 440:1222–1226. [PubMed: 16642001]

Ganguly KK, Pal S, Moulik S, Chatterjee A. Integrins and metastasis. Cell adhesion & migration. 2013; 7:251–261. [PubMed: 23563505]

Hartman GD, Egbertson MS, Halczenko W, Laswell WL, Duggan ME, Smith RL, Naylor AM, Manno PD, Lynch RJ, Zhang G, et al. Non-peptide fibrinogen receptor antagonists. 1. Discovery and design of exosite inhibitors. Journal of medicinal chemistry. 1992; 35:4640–4642. [PubMed: 1469694]

Hay ED. Extracellular matrix. The Journal of cell biology. 1981; 91:205s–223s. [PubMed: 6172429]

Hay ED. Extracellular matrix, cell skeletons, and embryonic development. American journal of medical genetics. 1989; 34:14–29. [PubMed: 2683777]

Heukamp LC, Thor T, Schramm A, De Preter K, Kumps C, De Wilde B, Odersky A, Peifer M, Lindner S, Spruessel A, et al. Targeted expression of mutated ALK induces neuroblastoma in transgenic mice. Science translational medicine. 2012; 4:141ra191.

Huth J, Buchholz M, Kraus JM, Schmucker M, von Wichert G, Krndija D, Seufferlein T, Gress TM, Kestler HA. Significantly improved precision of cell migration analysis in time-lapse video microscopy through use of a fully automated tracking system. BMC cell biology. 2010; 11:24. [PubMed: 20377897]

Hynes RO. Integrins: bidirectional, allosteric signaling machines. Cell. 2002; 110:673–687. [PubMed: 12297042]

Hynes RO, Naba A. Overview of the matrisome--an inventory of extracellular matrix constituents and functions. Cold Spring Harbor perspectives in biology. 2012; 4:a004903. [PubMed: 21937732]

Junqueira LC, Cossermelli W, Brentani R. Differential staining of collagens type I, II and III by Sirius Red and polarization microscopy. Archivum histologicum Japonicum = Nihon soshikigaku kiroku. 1978; 41:267–274. [PubMed: 82432]

Kagan HM, Li W. Lysyl oxidase: properties, specificity, and biological roles inside and outside of the cell. Journal of cellular biochemistry. 2003; 88:660–672. [PubMed: 12577300]

Kim D, Pertea G, Trapnell C, Pimentel H, Kelley R, Salzberg SL. TopHat2: accurate alignment of transcriptomes in the presence of insertions, deletions and gene fusions. Genome biology. 2013; 14:R36. [PubMed: 23618408]

Kimmel CB, Ballard WW, Kimmel SR, Ullmann B, Schilling TF. Stages of embryonic development of the zebrafish. Developmental dynamics : an official publication of the American Association of Anatomists. 1995; 203:253–310. [PubMed: 8589427]

Kirschmann DA, Seftor EA, Fong SF, Nieva DR, Sullivan CM, Edwards EM, Sommer P, Csiszar K, Hendrix MJ. A molecular role for lysyl oxidase in breast cancer invasion. Cancer research. 2002; 62:4478–4483. [PubMed: 12154058]

Kurozumi A, Goto Y, Matsushita R, Fukumoto I, Kato M, Nishikawa R, Sakamoto S, Enokida H, Nakagawa M, Ichikawa T, Seki N. Tumor-suppressive microRNA-223 inhibits cancer cell migration and invasion by targeting ITGA3/ITGB1 signaling in prostate cancer. Cancer science. 2016; 107:84–94. [PubMed: 26509963]

Langenau DM, Keefe MD, Storer NY, Jette CA, Smith AC, Ceol CJ, Bourque C, Look AT, Zon LI. Co-injection strategies to modify radiation sensitivity and tumor initiation in transgenic Zebrafish. Oncogene. 2008; 27:4242–4248. [PubMed: 18345029]

Langmead B, Salzberg SL. Fast gapped-read alignment with Bowtie 2. Nature methods. 2012; 9:357–359. [PubMed: 22388286]

Lapointe J, Li C, Higgins JP, van de Rijn M, Bair E, Montgomery K, Ferrari M, Egevad L, Rayford W, Bergerheim U, et al. Gene expression profiling identifies clinically relevant subtypes of prostate cancer. Proceedings of the National Academy of Sciences of the United States of America. 2004; 101:811–816. [PubMed: 14711987]

Levental KR, Yu H, Kass L, Lakins JN, Egeblad M, Erler JT, Fong SF, Csiszar K, Giaccia A, Weninger W, et al. Matrix crosslinking forces tumor progression by enhancing integrin signaling. Cell. 2009; 139:891–906. [PubMed: 19931152]

Li XQ, Lu JT, Tan CC, Wang QS, Feng YM. RUNX2 promotes breast cancer bone metastasis by increasing integrin alpha5-mediated colonization. Cancer letters. 2016; 380:78–86. [PubMed: 27317874]

Lu X, Wan F, Zhang H, Shi G, Ye D. ITGA2B and ITGA8 are predictive of prognosis in clear cell renal cell carcinoma patients. Tumour biology : the journal of the International Society for Oncodevelopmental Biology and Medicine. 2016; 37:253–262. [PubMed: 26198048]

Lutz W, Stohr M, Schurmann J, Wenzel A, Lohr A, Schwab M. Conditional expression of N-myc in human neuroblastoma cells increases expression of alpha-prothymosin and ornithine decarboxylase and accelerates progression into S-phase early after mitogenic stimulation of quiescent cells. Oncogene. 1996; 13:803–812. [PubMed: 8761302]

Maris JM. Recent advances in neuroblastoma. The New England journal of medicine. 2010; 362:2202–2211. [PubMed: 20558371]

Maris JM. Recent advances in neuroblastoma. N Engl J Med. 2011; 362:2202–2211.

Maris JM, Hogarty MD, Bagatell R, Cohn SL. Neuroblastoma. Lancet. 2007; 369:2106–2120. [PubMed: 17586306]

Matthews JM, Lester K, Joseph S, Curtis DJ. LIM-domain-only proteins in cancer. Nature reviews Cancer. 2013; 13:111–122. [PubMed: 23303138]

Menke AL, Spitsbergen JM, Wolterbeek AP, Woutersen RA. Normal anatomy and histology of the adult zebrafish. Toxicologic pathology. 2011; 39:759–775. [PubMed: 21636695]

Miranti CK, Brugge JS. Sensing the environment: a historical perspective on integrin signal transduction. Nature cell biology. 2002; 4:E83–90. [PubMed: 11944041]

Naba A, Clauser KR, Hoersch S, Liu H, Carr SA, Hynes RO. The matrisome: in silico definition and in vivo characterization by proteomics of normal and tumor extracellular matrices. Molecular & cellular proteomics : MCP. 2012; 11:M111 014647.

Nagata M, Noman AA, Suzuki K, Kurita H, Ohnishi M, Ohyama T, Kitamura N, Kobayashi T, Uematsu K, Takahashi K, et al. ITGA3 and ITGB4 expression biomarkers estimate the risks of locoregional and hematogenous dissemination of oral squamous cell carcinoma. BMC cancer. 2013; 13:410. [PubMed: 24006899]

Neely GG, Hess A, Costigan M, Keene AC, Goulas S, Langeslag M, Griffin RS, Belfer I, Dai F, Smith SB, et al. A genome-wide Drosophila screen for heat nociception identifies alpha2delta3 as an evolutionarily conserved pain gene. Cell. 2010; 143:628–638. [PubMed: 21074052]

Oldridge DA, Wood AC, Weichert-Leahey N, Crimmins I, Sussman R, Winter C, McDaniel LD, Diamond M, Hart LS, Zhu S, et al. Genetic predisposition to neuroblastoma mediated by a LMO1 super-enhancer polymorphism. Nature. 2015; 528:418–421. [PubMed: 26560027]

Park JR, Bagatell R, London WB, Maris JM, Cohn SL, Mattay KK, Hogarty M. Children's Oncology Group's 2013 blueprint for research: neuroblastoma. Pediatric blood & cancer. 2013; 60:985–993. [PubMed: 23255319]

Paszek MJ, Zahir N, Johnson KR, Lakins JN, Rozenberg GI, Gefen A, Reinhart-King CA, Margulies SS, Dembo M, Boettiger D, et al. Tensional homeostasis and the malignant phenotype. Cancer cell. 2005; 8:241–254. [PubMed: 16169468]

Pugh TJ, Morozova O, Attiyeh EF, Asgharzadeh S, Wei JS, Auclair D, Carter SL, Cibulskis K, Hanna M, Kiezun A, et al. The genetic landscape of high-risk neuroblastoma. Nat Genet. 2013

Qin L, Chen X, Wu Y, Feng Z, He T, Wang L, Liao L, Xu J. Steroid receptor coactivator-1 upregulates integrin alpha(5) expression to promote breast cancer cell adhesion and migration. Cancer research. 2011; 71:1742–1751. [PubMed: 21343398]

Renshaw SA, Trede NS. A model 450 million years in the making: zebrafish and vertebrate immunity. Disease models & mechanisms. 2012; 5:38–47. [PubMed: 22228790]

Smith-Mungo LI, Kagan HM. Lysyl oxidase: properties, regulation and multiple functions in biology. Matrix biology : journal of the International Society for Matrix Biology. 1998; 16:387–398. [PubMed: 9524359]

Smith SJ, Diehl NN, Smith BD, Mohney BG. Incidence, ocular manifestations, and survival in children with neuroblastoma: a population-based study. American journal of ophthalmology. 2010; 149:677–682. e672. [PubMed: 20149339]

Subramanian A, Tamayo P, Mootha VK, Mukherjee S, Ebert BL, Gillette MA, Paulovich A, Pomeroy SL, Golub TR, Lander ES, Mesirov JP. Gene set enrichment analysis: a knowledge-based approach for interpreting genome-wide expression profiles. Proceedings of the National Academy of Sciences of the United States of America. 2005; 102:15545–15550. [PubMed: 16199517]

Sweat F, Puchtler H, Rosenthal SI. Sirius Red F3ba as a Stain for Connective Tissue. Archives of pathology. 1964; 78:69–72. [PubMed: 14150734]

Tcheng JE, Talley JD, O'Shea JC, Gilchrist IC, Kleiman NS, Grines CL, Davidson CJ, Lincoff AM, Califf RM, Jennings LK, et al. Clinical pharmacology of higher dose eptifibatide in percutaneous coronary intervention (the PRIDE study). The American journal of cardiology. 2001; 88:1097–1102. [PubMed: 11703951]

Wang C, Gong B, Bushel PR, Thierry-Mieg J, Thierry-Mieg D, Xu J, Fang H, Hong H, Shen J, Su Z, et al. The concordance between RNA-seq and microarray data depends on chemical treatment and transcript abundance. Nature biotechnology. 2014; 32:926–932.

Wang K, Diskin SJ, Zhang H, Attiyeh EF, Winter C, Hou C, Schnepp RW, Diamond M, Bosse K, Mayes PA, et al. Integrative genomics identifies LMO1 as a neuroblastoma oncogene. Nature. 2011; 469:216–220. [PubMed: 21124317]

Wong CC, Tse AP, Huang YP, Zhu YT, Chiu DK, Lai RK, Au SL, Kai AK, Lee JM, Wei LL, et al. Lysyl oxidase-like 2 is critical to tumor microenvironment and metastatic niche formation in hepatocellular carcinoma. Hepatology. 2014; 60:1645–1658. [PubMed: 25048396]

Zhu S, Lee JS, Guo F, Shin J, Perez-Atayde AR, Kutok JL, Rodig SJ, Neuberg DS, Helman D, Feng H, et al. Activated ALK Collaborates with MYCN in Neuroblastoma Pathogenesis. Cancer cell. 2012; 21:362–373. [PubMed: 22439933]

Significance

Neuroblastoma is an embryonal tumor of the peripheral sympathetic nervous system that is widely disseminated at diagnosis and accounts for 10% of all pediatric cancer-related deaths. A genome-wide association study (GWAS) identified *LMO1* as a neuroblastoma susceptibility gene that is upregulated in high-risk neuroblastoma. Using our zebrafish model of tumorigenesis, we substantiate the role of LMO1 in the initiation and progression of neuroblastoma, demonstrating that the oncogenic mechanism is an increase in neuroblast cell proliferation during tumor initiation. Coexpression of *LMO1* and *MYCN* also deregulates genes promoting tumor cell-extracellular matrix interaction, leading to metastasis.

Highlights

1. Coexpression of *LMO1* with *MYCN* promotes neuroblastomagenesis.
2. Transgenic expression of LMO1 promotes neuroblastoma metastasis *in vivo*.
3. Increased LMO1 expression enhances neuroblastoma cell invasion and migration.
4. Increased LMO1 expression upregulates genes affecting tumor cell-matrix interactions.

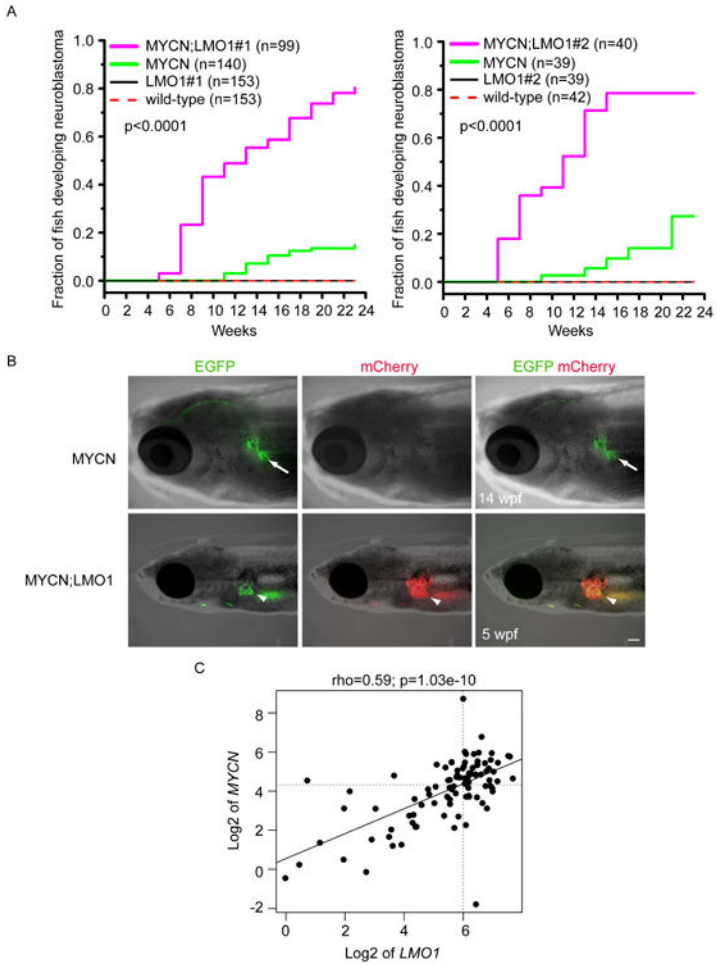

Figure 1. Coexpression of LMO1 and MYCN is associated with an earlier onset and increased penetrance of neuroblastoma

(A) Kaplan-Meier analysis of the cumulative frequency of neuroblastoma development over 6 months in stable transgenic zebrafish lines. MYCN represents heterozygous stable transgenic fish [*Tg*(*dβh:EGFP-MYCN*)]; LMO1#1 and LMO1#2 represent two individual heterozygous stable transgenic fish line [*Tg*(*dβh:LMO1),Tg*(*dβh:mCherry*) line #1 and #2]. The differences in cumulative frequency of neuroblastoma between MYCN-only transgenic fish and MYCN;LMO1#1 or #2 transgenic fish is statistically significant ($p<0.0001$, by the log-rank test).

(B) *Top*: MYCN transgenic fish with EGFP-expressing tumor (arrows) at 14 weeks post fertilization (wpf). *Bottom*: MYCN;LMO1 transgenic fish with EGFP and mCherry-expressing tumor (arrowheads) at 5 weeks post fertilization (wpf). Scale bar, 1 mm.

(C) Spearman's correlation analysis of *LMO1* and *MYCN* expression in high-risk neuroblastomas with single-copy *MYCN*. Data were derived from TARGET RNAseq cohort, the Sequence Read Archive (SRA) study accession phs000467. See also Figure S1.

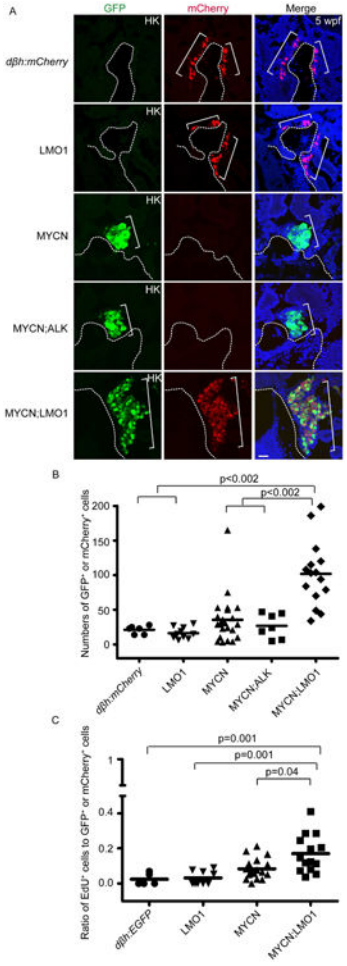

Figure 2. Transgenic expression of LMO1 promotes MYCN-induced hyperplasia of sympathoadrenal cells in the interrenal gland (IRG) at 5 weeks

(A) Sagittal sections through the IRG regions of the indicated transgenic fish at 5 wpf (dorsal up, anterior left). GFP, green; mCherry, red; Merge, combined green, red and blue. MCherry^{+}/GFP^{+}sympathoadrenal cells are indicated by brackets. Dotted lines indicate the head kidney (HK)boundary. Scale bar, 10 μm.

(B) Comparison of numbers of mCherry^{+} or GFP^{+} sympathoadrenal cells in the IRG of *dβh:mCherry*, LMO1, MYCN, MYCN;ALK and MYCN;LMO1 transgenic fish at 5 wpf.

(C) Ratio of EdU-labeled sympathoadrenal cells to the total number of GFP^{+} or mCherry^{+} sympathoadrenal cells in *dβh:EGFP*, MYCN, LMO1, and MYCN;LMO1 transgenic fish at 5 weeks.

Data are mean values of minimum five fish per group (B and C, horizontal bars). See also Figures S2 and S3.

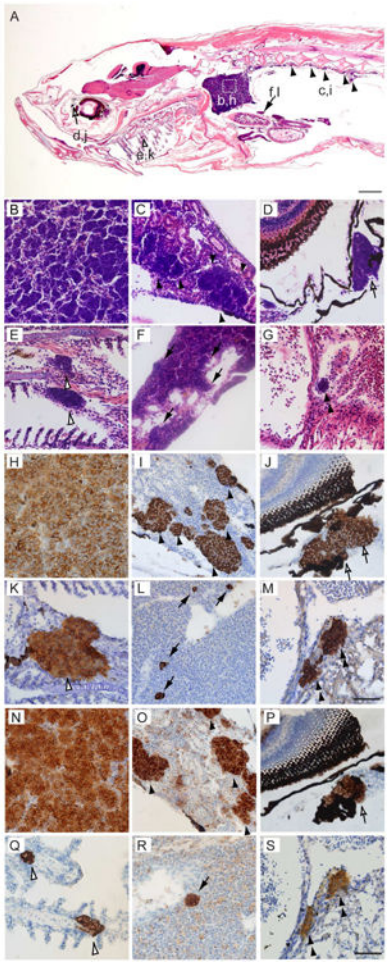

Figure 3. Coexpression of LMO1 and MYCN promotes distant metastases of neuroblastoma

(A-G) H&E-stained sagittal sections of MYCN;LMO1 transgenic fish at 6 months of age. (H-S) Immunohistochemical analyses of the sagittal sections of MYCN;LMO1 transgenic fish in magnified views, using tyrosine hydroxylase (TH) antibody (H-M) or GFP antibody (N-S). White box outlines the interrenal gland (b, h), magnified in panels B, H and N. Disseminated tumor cells were detected in the kidney marrow (c, i, C, I and O, solid black arrowheads), the sclera of the eye (d, j, D, J and P, open arrow), the gill (e, k, E, K and Q, open arrowhead), the spleen (f, l, F, L and R, solid black arrow), and the heart chamber (G, M and S, double arrowheads). Scale bars, 100 μm (A) and 50 μm (B-S). See also Figure S4.

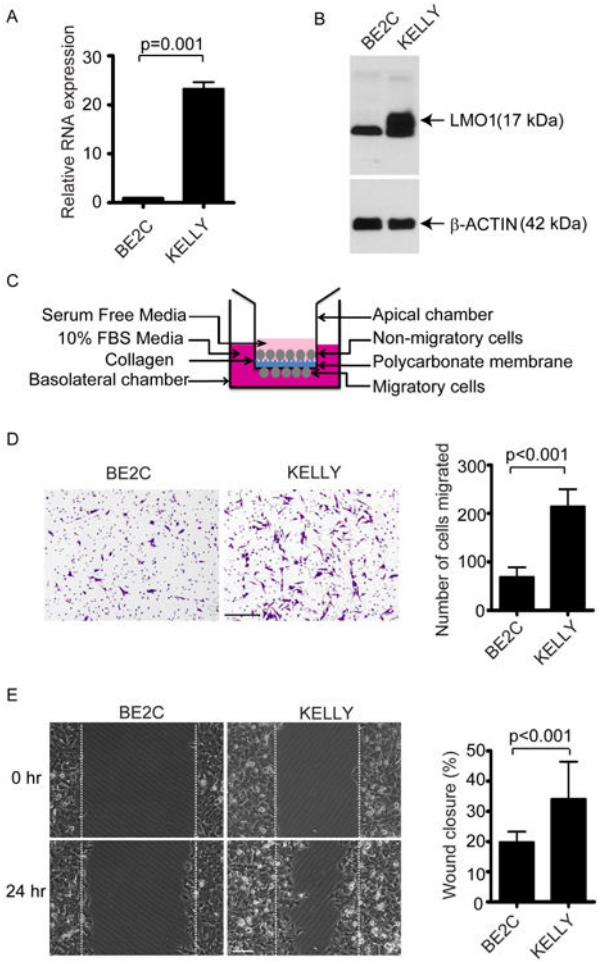

Figure 4. Increased LMO1 expression promotes the invasive and migratory properties of human neuroblastoma cells

(A) Relative expression of *LMO1* to *ACTIN* in the BE2C and Kelly cell lines, by semi-quantitative RT-PCR analysis.

(B) Immunoblot of LMO1 expression (arrow) in the BE2C and Kelly cell lines. The levels of ACTIN expression serve as loading control.

(C) Schematic diagram of transwell invasion and migration assay.

(D) Transwell invasion and migration assay of the BE2C and Kelly cell lines. Left: Crystal violet-stained migrated cells. Right: Number of migrated cells through the membrane per field (real number). Scale bar, 200 μm.

(E) Wound-healing assay of the BE2C and Kelly cell lines. Left: representative brightfield pictures of cells at 0 or 24 hour (hr) time-point. Right: quantification of cells migrated into wound area. Scale bar, 200 μm. Data are represented as mean ± SD of triplicate experiments (A, D and E). See also Figure S5.

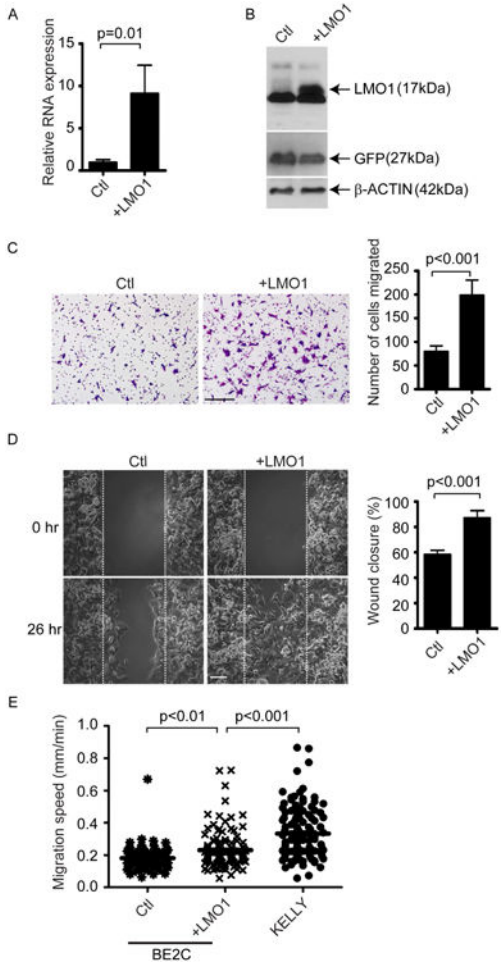

Figure 5. Increased LMO1 expression in BE2C cells promotes cell invasion and migration

(A) Q RT-PCR analysis of LMO1 expression in the BE2C cells with stable overexpression of LMO1 (+LMO1) or control vector (Ctl).

(B) Immunoblot of LMO1 (arrow) and control GFP expression in the BE2C cells with stable overexpression of LMO1 (+LMO1) or control vector (Ctl). The levels of GFP and ACTIN expression serve as loading control.

(C) Transwell migration assay of the BE2C cells with overexpression of LMO1 (+LMO1) or control vector (Ctl). Left: Crystal violet-stained migrated cells. Right: Number of migrated cells through the membrane per field (real number). Scale bar, 200 μm.

(D) Wound-healing assay of the BE2C cells with overexpression of LMO1 (+LMO1) or control vector (Ctl). Left: representative brightfield pictures of cells at 0 or 26 hour (hr) time-point. Right: quantification of migrated cells into wound area. Scale bar, 200 μm. The data are represented as mean ± SD of triplicate experiments (A, C and D).

(E) Comparison of the speed of random migration of human neuroblastoma cell lines, including BE2C cells with stable overexpression of LMO1 (+LMO1) or control vector (Ctl) and Kelly cells. Mean values (horizontal bars) were compared by One-way ANOVA with Tukey's post-hoctest.

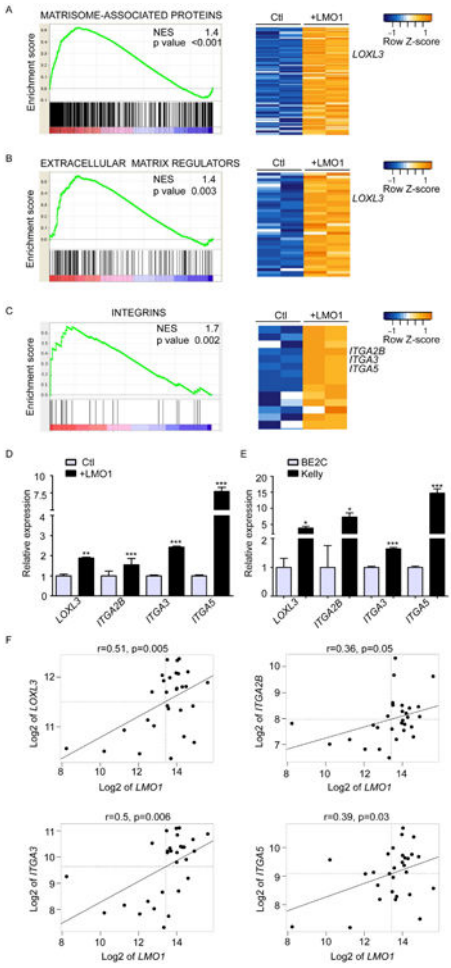

Figure 6. Increased LMO1 expression upregulates genes affecting tumor cell-ECM interaction

(A-C) Left panels: GSEA of the gene expression profile of BE2C cells with stable overexpression of LMO1 (+LMO1) or control vector (Ctl). Representative significantly enriched gene signatures include the matrisome-associated proteins (A, NABA Matrisome-Associated gene set, p<0.001), extracellular matrix regulators (B, NABA ECM Regulators gene set, p=0.003) and integrins (C, HGNC INTEGRIN Family, p=0.002). Genes are ranked by score and plotted on the x-axis by vertical black bars, and the normalized enrichment score is plotted in green. Right panels: Heat maps of the expression of genes that constitute to the given processes. Each row corresponds to a gene whose expression is normalized across the row. Representative enriched genes that subjected for qRT-PCR analysis are marked in the heat maps.

(D,E) Relative expression values of the representative genes identified from enriched biological processes in LMO1-expressing (+LMO1) vs. vector-expressing control (Ctl) BE2C cells (D), or in Kelly vs. BE2C cells (E) by qRT-PCR analyses. All the values were further normalized to the mean of each given gene in the vector-expressing control BE2C cells (D) or in the BE2C parental cells (E). The data are represented as mean ± SD of triplicate experiments; * p<0.05, **p<0.01 and ***p<0.001 by two-tailed t-test.

(F) Correlation analyses between *LMO1* and *LOXL3*, *ITGA2B*, *ITGA3*, or *ITGA5* expression in stage 4 neuroblastomas with single-copy *MYCN*. Data were derived from

Westermann-105-custom-ag44kcwolf microarray expression data GSE73517. See also Figure S6.

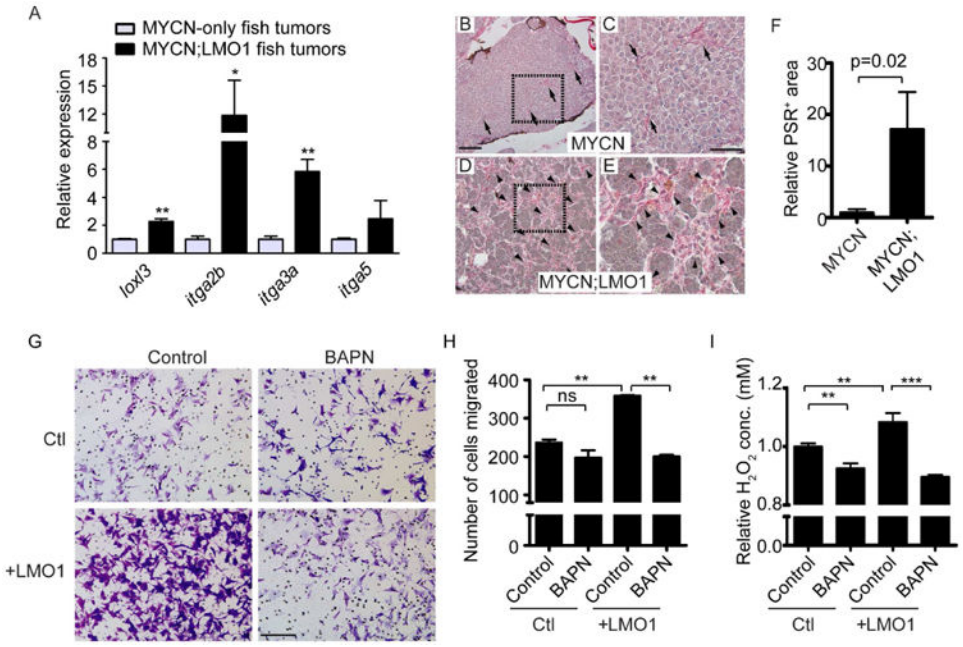

Figure 7. Increased LMO1 expression promotes collagen deposition and LOX-dependent cell migration and invasion

(A) Relative expression values of *loxl3*, *itga2b*, *itga3*, and *itga5* to *elfa* in neuroblastoma from three MYCN-only or three MYCN;LMO1 transgenic fish by qRT-PCR analysis. All the values were further normalized to the mean of each given gene in MYCN-only tumors. The data are represented as mean ± SD; *p<0.05 and **p<0.01 by two-tailed t-test.

(B-E) Representative light microscopy images of picrosirius red (PSR)-stained collagen fibers on the tumor sections from MYCN-only (B, C) or MYCN;LMO1 (D, E) transgenic fish. Boxed area in B and D were magnified in C and E, with arrows (B, C) and arrowheads (D, E) indicating the PSR-positive collagen fibers, respectively. Scale bars, 100 μm (B, D) and 50 μm (C, E).

(F) Quantification of PSR-stained area on MYCN-only or MYCN;LMO1 tumor sections. Results were normalized to the mean of PSR-stained area in MYCN-only tumors. The data are represented as mean ± SD of three MYCN-only or three MYCN;LMO1 tumors; p=0.02 by two-tailed t-test.

(G) Transwell migration assay of the BE2C cells with overexpression of LMO1 (+LMO1) or control vector (Ctl) in the absence (Control) or presence of LOX inhibitor BAPN (500 μM) (BAPN). Scale bar, 200 μm.

(H) Quantification (real number) of migrated cells through the membrane per field in (G).

(I) Amplex Red assay to determine LOX enzymatic activity in media of the control (Ctl) or LMO1-expressing (+LMO1) BE2C cells with or without treatment of BAPN. Data are represented as mean ± SD of triplicate experiments (H and I), **p<0.01 and ***p<0.001 by one-way ANOVA with Tukey's post-hoc test.

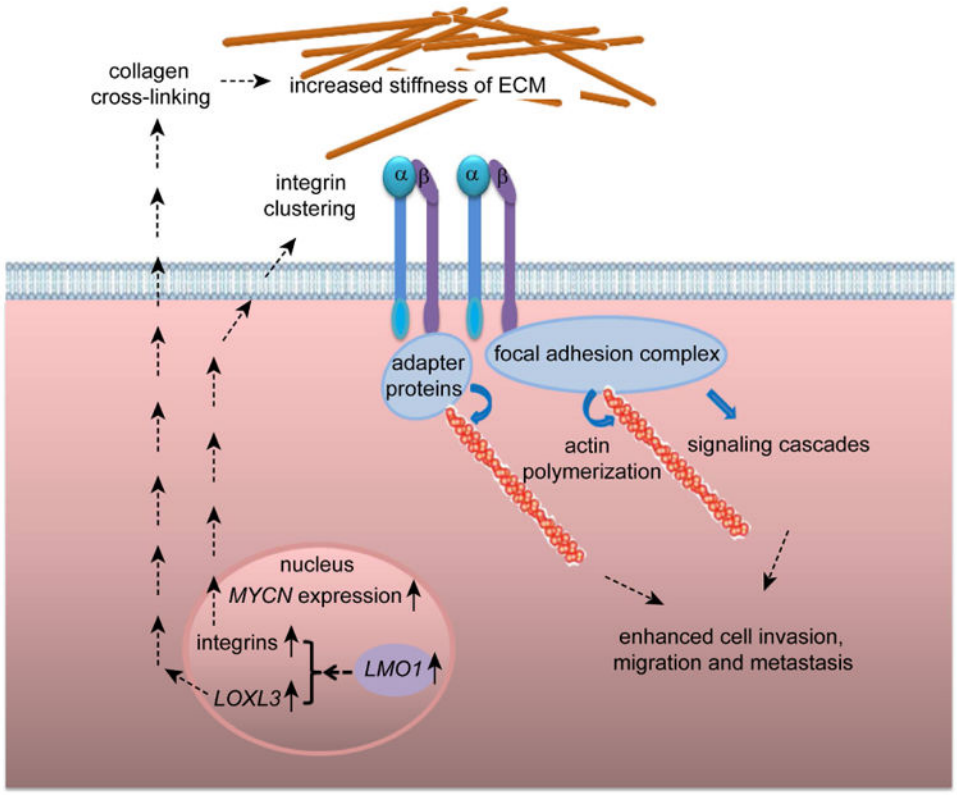

Figure 8. Hypothetical model for the synergy between LMO1 and MYCN in neuroblastoma metastasis

When neuroblastoma cells coexpress high levels of *MYCN* and *LMO1*, the expression of ECM regulator genes, including *LOXL3*, *ITGA2B*, *ITGA3*, and *ITGA5*, is upregulated. This could lead to the remodeling of extracellular matrix, the assembly of focal adhesion complexes, and the rearrangement of actin cytoskeleton, subsequently resulting in enhanced invasion, motility and metastasis of these neuroblastoma cells.